Sub-nanoscale, single-molecule, magnetic–electronic switching from externally perturbed spin states in iron (III)-based complexes

2005 J. Phys.: Condens. Matter 17 S727

(http://iopscience.iop.org/0953-8984/17/11/002)

INSTITUTE OF PHYSICS PUBLISHING JOURNAL OF PHYSICS: CONDENSED MATTER

J. Phys.: Condens. Matter **17** (2005) S727–S742 doi:10.1088/0953-8984/17/11/002

Sub-nanoscale, single-molecule, magnetic–electronic switching from externally perturbed spin states in iron (III)-based complexes

G R Hearne[1], O Munro[2], N Pearson[2] and M Shongwe[3]

[1] School of Physics, University of the Witwatersrand, PO Wits 2050, Johannesburg-Gauteng, South Africa
[2] School of Chemical and Physical Sciences, University of Kwazulu-Natal, Private Bag X01, Pietermaritzburg 3209, South Africa
[3] Department of Chemistry, College of Science, Sultan Qaboos University, PO Box 36, Postal Code 123, Al-Kodh, Sultanate of Oman

Received 5 January 2005
Published 4 March 2005
Online at stacks.iop.org/JPhysCM/17/S727

Abstract

Both the temperature and pressure dependent spin state transition behaviour of two Fe(III) complexes will be exemplified. Such compounds are considered attractive as potential molecular switch devices for low power, low weight, high density nanomemory arrays in computer applications, or as sensors. Spin state configurations are readily investigated by ^{57}Fe Mössbauer spectroscopy in the range 300–4 K, or at high pressures up to 20 GPa in diamond anvil cells.

An iron coordination compound with the chemical formula $\{[Fe^{III}L_2][ClO_4]\}_2{\cdot}EtOH$, where L^- is a uni-negative ligand, HL is *N*-(pyridin-2-ylmethyl)salicylideneamine and EtOH is ethanol, is in the high spin (HS), $^6A_{1g}$, state at room temperature. The onset of low spin (LS) population occurs at ∼240 K and this increases monotonically as the temperature is lowered to 100 K. At 70 K the sample is predominantly in the LS state although a remnant ∼12% HS population persists to the lowest recorded temperature of ∼15 K. Thermodynamic parameters associated with the energy barrier between the two spin states are deduced from the temperature dependence of the equilibrium constant K.

Pressure induced spin switching from the high moment HS state to the low moment LS electronic state in a haem-porphyrin $[Fe^{III}(TPP)(NCS)]$ will also be shown. Spin pairing onset occurs at a moderate pressure of ∼5 GPa. HS and LS isomers exist in equilibrium up to ∼12 GPa at room temperature. The sample is fully LS populated at $P > 12$ GPa. Temperature and pressure dependent spin–spin relaxation is used to account for the pressure evolution of the (asymmetric) quadrupole split resonance profile. Density functional theory calculations, in conjunction with crystallographic data, are used to consider the structural response to such a spin state variation, perhaps suggesting the possibility of a mechanically operated single-molecule magnetic switch.

(Some figures in this article are in colour only in the electronic version)

1. Introduction

The idea of finding ever more miniature electronic components is considered imperative for high density computing, data storage and information technology. Nanomaterials have attracted considerable attention in this regard, where typical dimensions are in the range of several nanometres up to tens of nanometres. However, there has also been considerable research in recent years on exploiting possible electronic switching characteristics of single molecules or of an assembly of molecules [1]. Such a switching possibility is known as electronic bistability—the ability of a molecular species to exist in different electronic states at the same temperature, driven by an external perturbation, e.g., pressure [2] or light irradiation [3]. These would then constitute sub-nanoscale devices able to open up an exciting area of molecule-based electronics, now aptly termed *molectronics*. The most promising candidates for fabrication of such devices are spin transition complexes [2, 4], which are often molecular systems of transition metal compounds with medium ligand field strength and a 3d electronic configuration between d^4 and d^7. There are a number of iron-based complexes in this category, although it has been predominantly Fe(II):$3d^6$ complexes that have exhibited such bistability, driven by external perturbations of temperature, pressure and light irradiation. Typically in such systems the spin transition is from the high spin (HS) ionic spin $S = 2$ to the low spin (LS) $S = 0$ diamagnetic state. By contrast to this, there are hardly any examples of a corresponding spin state transition occurring in Fe(III) molecular complexes ($S = 5/2 \rightarrow 1/2$). In this work we will show two such examples of spin state transitions in Fe(III) complexes, driven by temperature and pressure. Ligands have been appropriately chosen in these complexes to ensure that (HS/LS) $^6A_{1g} \leftrightarrow ^2 T_{2g}$ interconversion occurs under relatively moderate thermodynamic (T or P) conditions.

The first Fe(III) complex to be considered is an iron coordination compound $\{[FeL_2][ClO_4]\}_2 \cdot EtOH$ (L^- is a uni-negative ligand, where HL = *N*-(pyridin-2-ylmethyl)salicylideneamine; EtOH = ethanol; molar mass of 1201.62 g mol^{-1}) which has recently been characterized by single-crystal x-ray crystallography. For this compound (hereafter denoted as $\{[Fe(Salpm)_2][ClO_4]\}_2 \cdot EtOH$), there are two complex cations in the same unit cell which are indistinguishable in the Mössbauer spectrum at room temperature. For each cation there are two deprotonated tridentate ligands *coordinated* with the iron (III) ion at the centre by the donor (electron-rich) atoms: a phenolate oxygen, an imine nitrogen and a pyridyl nitrogen, to form a mononuclear octahedral complex; see figure 1. The donor set FeO_2N_4 provides a ligand field strength that favours the occurrence of the (HS/LS) $^6A_{1g} \leftrightarrow ^2T_{2g}$ interconversion. Preliminary variable temperature x-ray analysis, from room temperature down to 150 K, has suggested coexistence of the HS and LS states in this Fe(III) complex.

The second Fe(III) complex that will be considered is a haem-porphyrin. Porphyrins have in common a substituted *macrocyclic ring* consisting of four pyrrole rings linked by four methane bridging groups; see figure 2. They are nominally flat stable molecules but there are numerous derivatives in which the macrocycle becomes buckled with major distortions from planarity. The hole in the middle of the macrocycle can complex with a large variety of metal ions, including iron, through the pyrrole nitrogens. The main function of porphyrins in living and synthetic systems is to complex with metal ions which act as centres for significant biological events. Only small variations on the basic structural theme of porphyrins lead to a wide variety of biological functions [5]. Two pertinent examples of where porphyrins are found in Nature are in haem (found in haemoglobin and myoglobin) and cytochrome *c*. Normally upon binding with oxygen, iron irreversibly changes its oxidation state, but the combination of porphyrin ligand and protein environment in the case of haem proteins changes the redox potential of the Fe ion and its oxidation becomes reversible. In cytochrome *c* the iron cycles

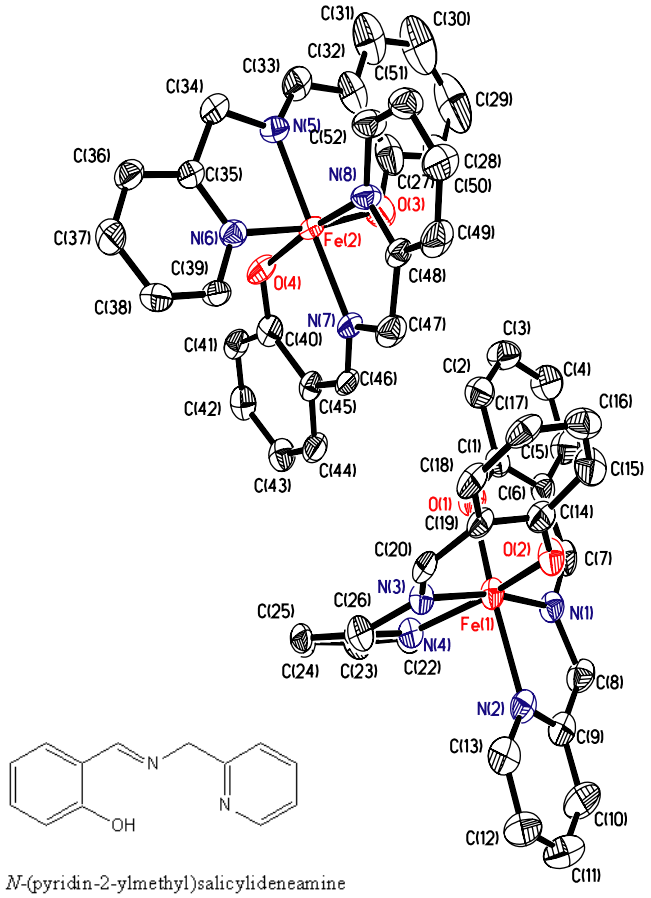

Figure 1. An ORTEP diagram of thermal ellipsoids (displaying selected atom labels) of the x-ray structure determined at 150 K for $\{[Fe(Salpm)_2][ClO_4]\}_2 \cdot EtOH$ considered in this work. To balance the charge, a perchlorate ion crystallizes with the complex cation. There is also an ethanol ($EtOH{=}CH_3CH_2OH$) molecule in the unit cell. The ClO_4^- and ethanol molecule have not been included in the diagram. Ethanol is the solvent from which the complex was crystallized. Shown are the two molecules involving HS Fe(1) and LS Fe(2) found in the same unit cell at the same temperature. Two ligands are coordinated with each metal ion and the ligand involved is shown in the inset.

through the 2+ and 3+ oxidation states while performing the function of electron transfer in cell respiration.

In the case of the Fe(III) porphyrin, [Fe(TPP)(NCS)], studied in this work the iron is complexed in a haem. The porphinato ring itself is four coordinate and in addition a fifth thiocyanate (NCS) axial ligand is coordinated with the central iron ion; see figure 2. For this five-coordinate Fe(III) (nominally $3d^5$), the metal is HS ($S = 5/2$) with large out of plane displacements for weak ligands, and LS with strong ligands with the metal in or near the porphine plane. Single-crystal XRD data at room temperature reveal the average Fe–N_p (planar) bond distance to be 2.067(2) Å and the Fe–N_{ax} (axial) bond distance is 1.936(3) Å. The coordination group of the iron in the [Fe(TPP)(NCS)] molecule is square pyramidal (C_{2v} symmetry), characteristic of five-coordinate metalloporphyrins [6]. There is a perpendicular displacement of 0.553 Å of the iron (III) ion from the least squares plane of the 24-atom

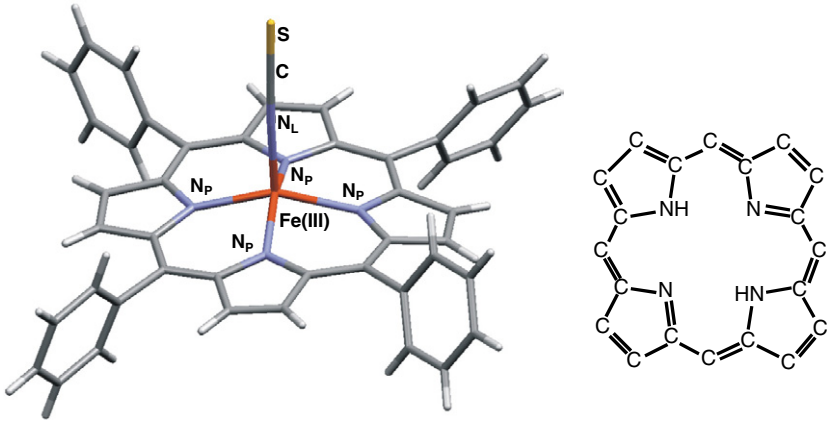

Figure 2. A diagram (displaying selected atom labels) of the room temperature x-ray structure of the haem-porphyrin [Fe(TPP)(NCS)]. Hydrogen atoms have been omitted for clarity. An axial thiocyanate ligand extends perpendicular to the porphyrin plane. The inset shows the macrocyclic porphyrin core that normally complexes with the metal cation.

porphyrin core (arising from a size mismatch), well within the range of 0.39–0.60 Å expected for a HS Fe(III) ion.

2. Experimental section

The mononuclear complex of iron (III) $\{[Fe(Salpm)_2][ClO_4]\}_2{\cdot}EtOH$ [HSalpm = *N*-(pyridin-2-ylmethyl)salicylideneamine] was isolated as black crystals from the template reaction of salicylaldehyde, the appropriate primary amine and iron (III) perchlorate hexahydrate in stoichiometric amounts. X-ray crystallography revealed the pseudo-octahedral coordination geometry at the metal centres with meridional and *cis, cis, trans* arrangements of the donor atoms.

A 60% enriched sample of [^{57}Fe(TPP)(NCS)] was synthesized for Mössbauer experiments and full details of the synthesis procedure will be published elsewhere. Briefly, isotopically enriched $FeCl_2$ was synthesized from iron filings (0.36 mmol, 2 mg) and ^{57}Fe metal pellets (0.53 mmol, 3 mg) added to 5M HCl (25 ml), degassed and under nitrogen. The $^{57}FeCl_2$ extracted from this process was then combined with TPP (*meso*-5,10,15,20-tetraphenylporphyrin dianion, 0.107 mmol, 44 mg) to first form [^{57}Fe(TPP)Cl]. This was combined with [K(18-crown-6)(NCS)] to form a solution layered under hexane. All synthesis procedures were carried out under dry nitrogen or *in vacuo*. X-ray quality crystals were obtained after five days. The unit cell parameters were equivalent within experimental error to those obtained for [Fe(TPP)(NCS)].

Temperature dependent measurements of the powdered Fe(III) coordination compound have been conducted in a Janis cryostat, where temperature stability can be maintained at better than 1 K for $T > 40$ K, and to 0.1 K at temperatures below this, using a Lakeshore temperature controller and calibrated Si diode thermometer. In this case a conventional ^{57}Co(Rh) source ($\sim$30 mCi) has been used. Pressure measurements, mainly at room temperature, have been performed in a Merrill–Basset-type diamond anvil cell (DAC) on the ^{57}Fe-enriched Fe(III) porphyrin which has been synthesized in milligram quantities. This sample was crushed into a powder and loaded into a 300 μm diameter cavity drilled in a TaW gasket. Some fine ruby powder was also added to permit pressure determination from the ruby fluorescence line shift.

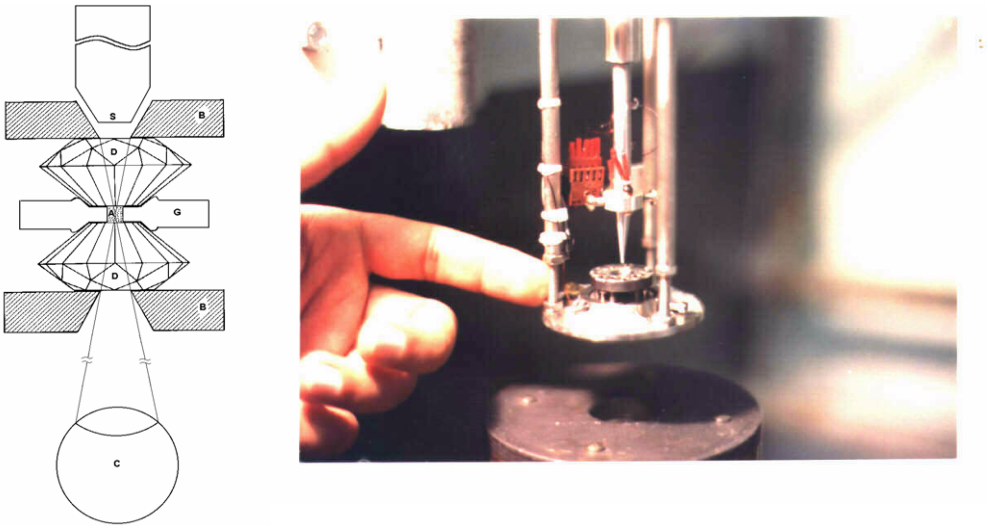

Figure 3. A schematic diagram of the experimental set-up for ^{57}Fe Mössbauer pressure measurements in the DAC: A is the sample cavity ($\varnothing \sim 300\ \mu$m), B is the diamond anvil support, C is the detector, D is the diamond anvil, G is the TaW metal gasket and S is the γ-ray 'point' source.

Liquid nitrogen was also loaded into the cavity as a pressure transmitting medium. In this case a 'point' ^{57}Co(Rh) source [7] (5–10 mCi) has been used; see figure 3. For selected measurements at both low temperature and elevated pressure this pressurized assembly has been loaded into the cryostat station described above.

3. The effect of temperature on an Fe(III) coordination compound, $\{[Fe(Salpm)_2][ClO_4]\}_2\cdot EtOH$

3.1. The temperature dependence of the Mössbauer spectra

Fe(III) compounds and the associated $3d^5$ orbital population typically have asymmetry parameters (quadrupole splitting) $\Delta E_Q < 1$ mm s^{-1} when in the HS state, because of the highly symmetric $^6S_{5/2}$ electronic configuration. Figure 4 and the fitted parameters ($\Delta E_Q = 0.71$ mm s^{-1}, $IS_{Fe} = 0.39$ mm s^{-1} at 300 K) show that $\{[Fe(Salpm)_2][ClO_4]\}_2\cdot EtOH$ is in the HS state at room temperature. The asymmetric doublet is attributed to spin–spin relaxation effects and a Boltzmann population of the Kramers doublets (Fe^{3+} ionic spin projection $S_z = \pm 1/2, \pm 3/2, \pm 5/2$) that originate from the spin–orbit split multiplet [8, 9]. This multiplet is from the lowest ionic level that arises from residual crystal field effects on the degenerate t_{2g} energies of the iron 3d orbitals. The asymmetric broadening of the resonance profile (e.g. the room temperature spectrum of figure 4) is explicable on the basis of an internal magnetic field B_{hf} originating from the resultant hyperfine interactions between the nucleus and s electrons polarized by the $S_z = \pm 5/2$ and $\pm 3/2$ d shell electrons. The B_{hf} sensed by the ^{57}Fe nucleus depends on the magnitude of the core polarization which in turn depends on S_z and the rapid relaxation (spin flip fluctuations) of the $S_z = \pm 1/2$ state. No magnetic hyperfine field B_{hf} will be observed at temperatures much below those characteristic of the energy gap D (1–10 cm^{-1}) between the S_z^2 levels when the $S_z = \pm 1/2$ state alone is occupied, near to liquid helium temperatures $T < 20$ K [8, 10]. This is because:

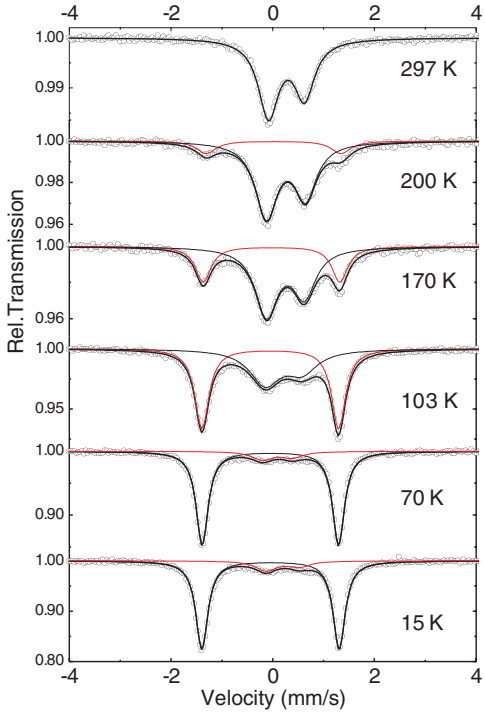

Figure 4. ^{57}Fe Mössbauer spectra of $\{[Fe(Salpm)_2][ClO_4]\}_2{\cdot}EtOH$ as a function of temperature upon warming from 10 K to room temperature. The solid line through the data (open circles) is the overall theoretical fit (sum of Lorentzian components). The inner doublet with unequal intensities is the HS component, predominant at high temperatures, whereas the wider doublet with equal intensities is supposed to be the LS population.

(i) the core polarization (and hence $B_{\rm hf}$) associated with the $S_z = \pm 1/2$ atomic spin projection is small; and

(ii) the relaxation times for this state are rapid compared to the inverse of the ^{57}Fe Larmor precession frequency (related to the sensing time of the Mössbauer nucleus), $\tau_{\rm R} \ll 1/\omega_{\rm L}$, and hence the time average of $B_{\rm hf}$ registers zero.

The LS signature is that of the wide *symmetric* doublet ($\Delta E_{\rm Q} = 2.68$ mm s^{-1}, $\mathrm{IS_{Fe}} = 0.19$ mm s^{-1} at 70 K) that is first seen in the spectrum at ∼200 K in figure 4. In this spin paired situation the atomic spin is $S = 1/2$ and there is only a single Kramers doublet $S_z = \pm 1/2$; the spin–spin relaxation is rapid and the core polarization is small so there is negligible magnetic hyperfine interaction, and a symmetric quadrupole doublet is obtained. This has a wide splitting $\Delta E_{\rm Q} \sim 2.7$ mm s^{-1} reflecting the large electric field gradient (EFG) which emanates from the asymmetric local electronic environment induced by the single unpaired spin of the LS state.

A plot of HS abundance as obtained from the integrated intensity (area) of the asymmetric doublet is shown in figure 5. This figure shows that HS and LS species coexist over quite a wide temperature range, 200–70 K, signifying non-cooperative spin equilibrium of the two states. As temperature is lowered from room temperature, the onset of the LS population first becomes manifested at ∼240 K. This is deduced by extrapolating from the linear regime in the range 200–70 K. There is a corresponding depopulation of the HS state as temperature is lowered beyond ∼240 K. However, there remains a ∼10% remnant HS population from 70 K down to

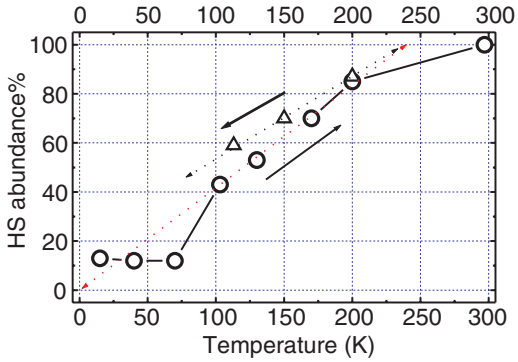

Figure 5. The HS contribution plotted as a function of temperature for the $\{[Fe(Salpm)_2][ClO_4]\}_2$·EtOH sample, as determined from the integrated area under the spectral component of the innermost asymmetric doublet of figure 1. Open circle symbols are measurements taken upon warming the sample and open triangle symbols, upon cooling the sample. Solid lines through the open circle symbols are to guide the eye. Dotted lines are through the temperature regimes where the abundance appears to change linearly with temperature. Extrapolation from this linear regime suggests that the onset of spin pairing is at ∼240 K. Note that ∼10 at.% of the iron remains HS down to the lowest recorded temperature. There appears to be a precipitous change in the HS population to this 10% plateau between 70 and 100 K.

the lowest temperature at which measurements have been made. This has precluded any need for further measurements at $T < 15$ K. The 10% HS remnant either represents an HS impurity phase masked by the HS majority phase at room temperature, or the remnant represents some constraint of the system of converting completely to the LS state at temperatures below ∼70 K.

3.2. Thermodynamic considerations

On the assumption that the spectra in figure 4 reflect an equilibrium mixture of HS and LS isomers, and α is the fraction of the LS isomer, the equilibrium constant K is [11, 12]

$$K = \left(\frac{\alpha}{1-\alpha}\right)(3\gamma)^{-1}\exp\left(\frac{E}{k_B T}\right). \tag{1}$$

k_B is the Boltzmann constant, E is the energy difference between the two spin states and γ is an entropy factor whose deviation from unity is indicative of the steepness of the gradual transition depicted in figure 5. That is, as γ deviates from unity, the transition becomes steeper. The equilibrium constant K at each temperature T is obtained from the HS and LS populations as derived from the relative areas of the sub-spectra in figure 4. A plot of $\ln(K)$ versus inverse temperature $1/T$ exhibits linearity, as shown in figure 6. This is considered evidence of an equilibrium mixture of the HS and LS species. The slope and intercept of the plot in figure 6 yield $E \sim 370$ K (i.e. 264 cm^{-1}) and $\gamma = 8$, respectively.

These permit us to derive thermodynamic quantities such as the change in enthalpy ΔH^0 and change in entropy ΔS^0 associated with the spin state transition:

$$\Delta H^0 = -NE, \tag{2}$$

$$\Delta S^0 = -R\ln(3\gamma), \tag{3}$$

where N and R are Avogadro's number and the gas constant, respectively.

The spin compensation temperature, where there is 50% population of HS and LS states, may be obtained from $T_c = \Delta H^0/\Delta S^0$. The thermodynamic parameters derived for warming and cooling have been listed in table 1.

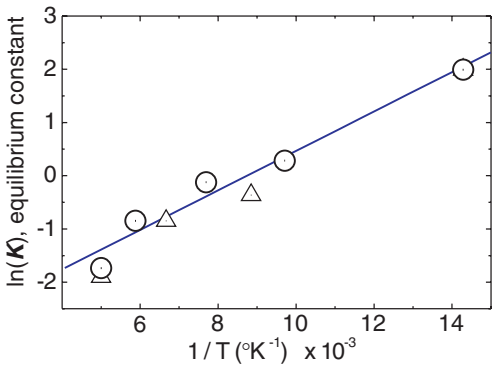

Figure 6. A plot of the logarithmic dependence of the equilibrium constant K on inverse temperature for the $[FeL_2][ClO_4]$·EtOH sample. The apparent linear dependence confirms the spin equilibrium situation that obtains in the range 200–70 K. Both the energy difference between the spin states and the entropy factor are obtained from the slope and intercept of a linear least squares fit to the data (the solid line through the data taken upon warming). Open circles are data taken upon warming and triangles are data taken upon cooling.

Table 1. Thermodynamic parameters derived for the sample $\{[Fe(Salpm)_2][ClO_4]\}_2$·EtOH from considerations of the spin equilibrium in the range 200–70 K.

	Warming	Cooling
E (K)	370	400
γ	8	15
ΔH^0 (cal mol^{-1})	−740	−790
ΔS^0 (cal mol^{-1} K^{-1})	−6.4	−7.6
T_c (K)	116	103

These may be compared with other systems, for example, ferric haemoprotein derivatives, for which such information is available, obtained from magnetic (paramagnetic susceptibility) measurements [12]. Such information for these iron coordination compounds may be useful in the design of molecular electronic switches, where the steepness (γ value) of the spin state transition and the onset temperature of the transition (related to T_c) need to be controlled, often by altering one of the surrounding ligands of the metal ion.

4. The effect of (temperature and) pressure on the Fe(III) molecular crystal [Fe(TPP)(NCS)]

4.1. Preliminary discussion

As yet, both the temperature and pressure dependence of the spin state of this compound, whose structure is depicted in figures 2 and 7, are not determined. Nor has the pressure dependence of the spin state of any other haem-porphyrin system been previously reported.

Understanding the crystal field splitting of a compound is critical to understanding and assigning its Mössbauer spectra. Figure 8 shows a crystal field energy diagram for conventional C_{4v} symmetry. The crystal field splitting is conventionally defined as the energy difference between d_{xy} and the $d_{x^2-y^2}$ orbitals.

By considering the DFT calculated coordination environment that surrounds the Fe(III) ion (details of which will be published elsewhere), we have noted that when the Fe(III)

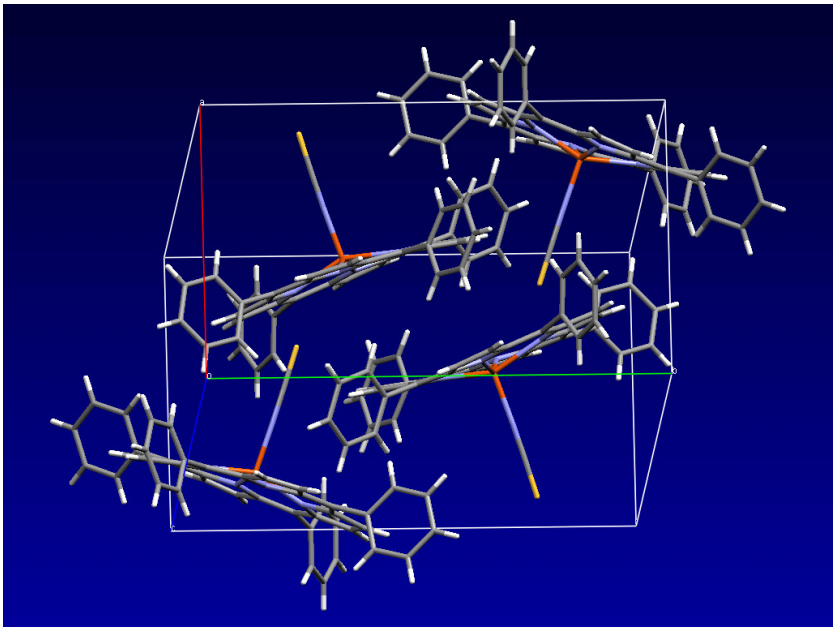

Figure 7. Shows how the molecules of [Fe(TPP)(NCS)] are arranged in the crystal unit cell. The molecules are stacked directly above one another to form columns which run parallel to the *a* axis. Each alternate column has its axial ligands facing in the opposite direction. The molecules within the columns are spaced such that the phenyl groups from neighbouring porphyrin molecules in adjacent columns are situated between them.

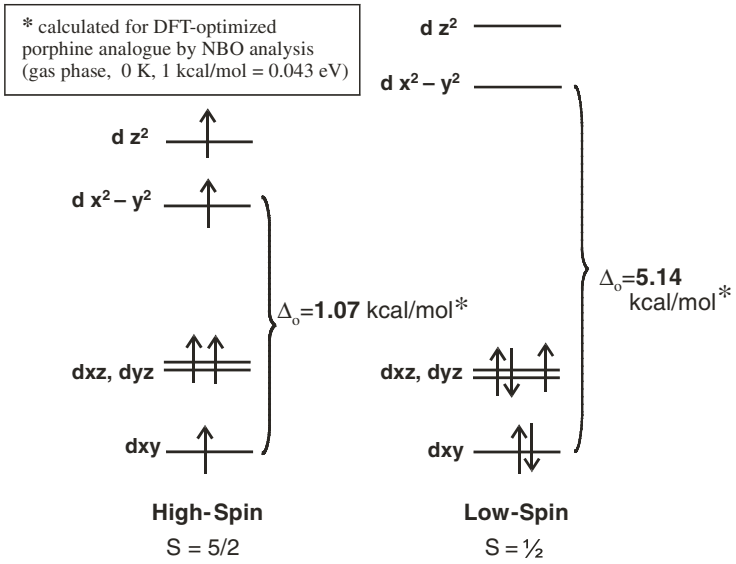

Figure 8. The crystal field energy diagram for conventional C_{4v} symmetry.

system switches from HS to LS, the predicted average Fe–N_p (planar) distance decreases from 2.097 to 2.009 Å (1.8% change) and the Fe–N_{ax} (axial) distance decreases from 1.924 to 1.891 Å (4.3%). This contraction of the coordination group causes more electron–electron

repulsion, thus changing the orbital energies, and results in a larger crystal field splitting in the LS state.

In a similar way, a decrease in temperature or an increase in pressure on a molecule in the HS state should lead to compression of the molecule and consequently contraction of the bond lengths. As the bond lengths are decreased and the coordinated metal ion is compressed, the crystal field splitting increases (figure 8) as a consequence of there being more and more electron repulsion between the nitrogen lone pair electrons and the 3d electrons of the Fe(III) ion that are involved in bonding. Eventually the energy needed to keep the two electrons in the e_g (d_{z^2} and $d_{x^2-y^2}$) orbitals (or the crystal field splitting) becomes larger than the energy required to overcome the spin pairing energy, and it is energetically favourable for 3d electrons to pair up and the complex crosses over to LS. When Fe(III) switches from HS to LS, there is a concomitant decrease in the radius of the ion as the $d_{x^2-y^2}$ and d_{z^2} orbitals become depopulated.

At the outset of the variable temperature study described herein, we were interested to see whether or not lowering the temperature would cause the bonds to contract sufficiently to cause [Fe(TPP)(NCS)] to switch from HS to LS; this kind of bond contraction has been observed in [Fe(TPP)(N_3)] [13].

4.2. Temperature dependent studies on [Fe(TPP)(NCS)]

In a low temperature x-ray study that was performed *after* the low temperature Mössbauer study, a 1.9% lattice contraction in the unit cell volume from room temperature down to 100 K was observed. Assuming that the relationship between temperature and cell volume remains linear, extrapolating down to 4 K gives only a 4% lattice contraction. On the basis of data in the literature for similar complexes [13], it was expected that lowering the temperature would induce *iron–nitrogen* bond contraction. However, in the low temperature x-ray structure of [Fe(TPP)(NCS)] the opposite was observed. The bond lengths show a very slight increase (within four standard deviations, and hence not experimentally significant) as the temperature is lowered. This study alone indicates that lowering the temperature is not sufficient to warrant a spin crossover in [Fe(TPP)(NCS)]. The DFT calculations also confirm that the HS state is the ground state for this compound.

The low temperature Mössbauer spectra of [Fe(TPP)(NCS)], in the order in which they were collected, are shown in figure 9. The isomer shifts (IS_{Fe}) for HS ferric complexes ($S = 5/2$) range from 0.27 to 0.49 mm s^{-1} and the quadrupole splittings ΔE_Q range from 0.46 to 1.89 mm s^{-1} [6, 14]. The Mössbauer spectra for [Fe(TPP)(NCS)] display a quadrupole doublet with a ΔE_Q of $\sim$0.4 mm s^{-1} and an IS_{Fe} of $\sim$0.2 mm s^{-1} in the temperature range 4.5–73 K.

For a HS d^5 metal ion in a symmetrical octahedral environment, the EFG would be zero, resulting in one symmetrical line in a Mössbauer spectrum. In the case of [Fe(TPP)(NCS)], there are five nitrogen atoms bonded to the Fe(III) ion in five out of the six sites available for perfect octahedral symmetry. For effective C_{4v} symmetry, there is a slight EFG due to the less than cubic symmetry of the system, which causes the doublet in the Mössbauer spectrum.

The quadrupole doublet that is present in the Mössbauer spectrum for [Fe(TPP)(NCS)] is not symmetrical throughout most of the temperature range 300–4 K. This asymmetry is rationalized in the same way as the asymmetric doublet of the iron coordination compound of the previous section, i.e., spin–spin relaxation effects and a Boltzmann population of the Kramers doublets (ionic spin projection $S_z = \pm 1/2, \pm 3/2, \pm 5/2$) that originate from the spin–orbit split multiplet derived from the axial crystal field split energy levels [8, 9].

The Mössbauer spectra confirm a relatively pure $S = 5/2$ ground state for [Fe(TPP)(NCS)] at temperatures up to 73 K. This is consistent with our DFT calculations which indicate that

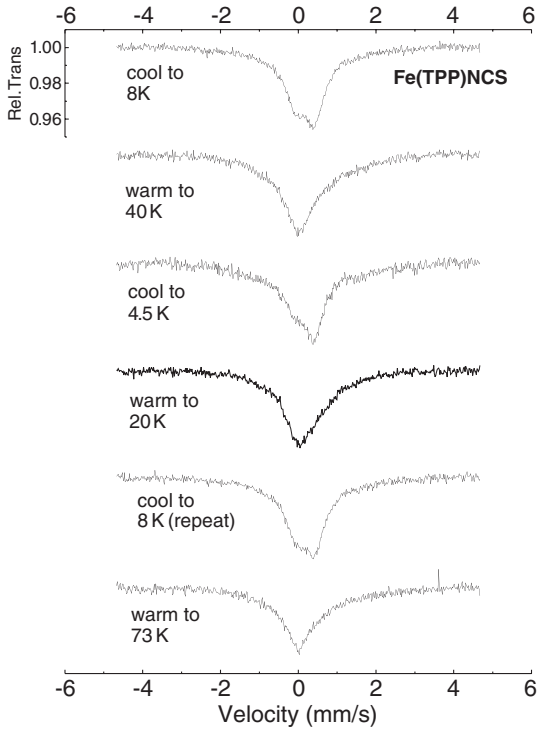

Figure 9. Sequential low temperature Mössbauer spectra obtained for [Fe(TPP)(NCS)].

the $S = 5/2$ state is the ground state and that the $S = 1/2$ state lies at considerably higher energy. There is no evidence of LS or intermediate spin states (i.e., $\Delta E_Q \sim 2$ mm s^{-1} and $\Delta E_Q \sim 3$ mm s^{-1}, respectively) mixing with the HS state.

4.3. Pressure dependent studies of [Fe(TPP)(NCS)]

By exerting a pressure in an anvil cell on soft molecular solids a unit cell volume reduction of up to ∼20% to 10 GPa may be achievable in some complexes [15]. This is a much larger contraction (∼5 times greater) than it is possible to induce with a temperature change (300 K → 4 K) and it is anticipated that this would be sufficient to induce a spin crossover in [Fe(TPP)(NCS)].

Two experimental runs to high pressures have been conducted. In the first run, the pressure was incremented in relatively small steps to locate the spin crossover pressure region, while the second run investigated the effect of extreme pressure on the sample by making large pressure increments, up to a highest pressure of 19.5 GPa.

The Mössbauer spectra collected from [^{57}Fe (TPP)(NCS)], in order of increasing pressure at room temperature as combined from both experimental runs, are shown in figure 10. It is evident that between ambient pressure and $P \sim 5.5$ GPa, from the quadrupole doublet ($\Delta E_Q \sim 0.4$ mm s^{-1}) and isomer shift, the bulk sample is HS. As the pressure is increased, some of the Fe(III) switches to the LS state. This is evidenced by the new quadrupole doublet that appears with $\Delta E_Q \sim 2$ mm s^{-1}. By $P \sim 7.2$ GPa, 33% of the sample is in the LS state and at 9.3 GPa, ∼62% of the sample is LS. The final two spectra recorded at 13.5 and 19.5 GPa clearly show that the [^{57}Fe (TPP)(NCS)] is fully LS from ∼13.5 GPa onwards and the LS state is maintained to higher pressures.

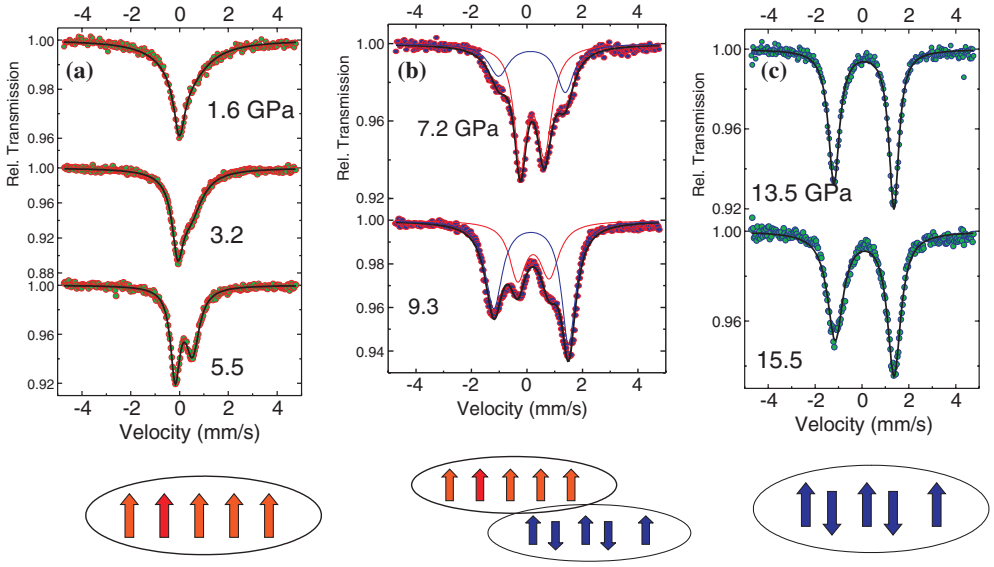

Figure 10. Mössbauer spectra recorded at room temperature for [^{57}Fe(TPP)(NCS)] in order of increasing pressure (in GPa); the three panels differentiate (a) the HS, (b) equilibrium HS/LS and (c) LS pressure regimes. In each spectrum the solid line through the data (filled circles) is the overall theoretical fit (sum of Lorentzian components).

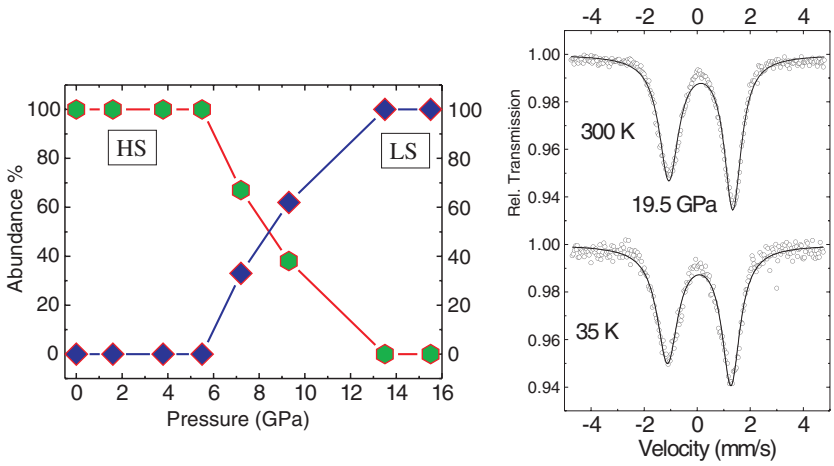

Figure 11. The left panel shows the percentage spin state change with compression. Filled diamonds correspond to the LS fraction. The right panel shows temperature dependent Mössbauer spectra recorded at the highest pressure of 19.5 GPa.

Figure 11 is a plot of the percentage spin state abundance for the ^{57}Fe(III) ion (HS or LS) with change in pressure. The plot simply shows that the spin transition is relatively gradual, and begins from about 5.5 GPa and is only complete at 13 GPa. From this plot we estimate P_c (where the HS/LS abundance is 50%) for [Fe(TPP)(NCS)] to be ∼8.5 GPa.

In the same figure 11 (right panel) we show the temperature behaviour of the spectra at the highest pressure of 19.5 GPa. When compared with the spectra taken in the HS state

of the low pressure regime (figure 10(a)), it may be noted that besides the wider quadrupole splitting indicative of the LS state, the asymmetry of the LS profile is reversed compared to the HS spectrum. In the LS state the lower nuclear transition energy (negative velocity) resonance is the less intense line, unlike in the case of the pure HS state up to ∼5 GPa. We first attempt an explanation of the behaviour of the spectra in the pure HS state up to ∼5.5 GPa, where the spectrum becomes progressively more symmetric as the pressure rises; see figure 10(a). Blume [8] has rationalized the temperature dependence of related compounds on the basis of temperature dependent spin–spin relaxation and the Boltzmann population of ionic energy levels ($S_z = \pm 1/2, \pm 3/2, \pm 5/2$ Kramers doublets) that arise from the spin–orbit coupling in an axial crystal field. As the temperature rises the spin flip (spin–spin relaxation) time τ_R in the spin–spin communication process increases, and the spectrum evolves from a more symmetric doublet at low T (<15 K) to an asymmetric profile at high T. As a function of increasing pressure, inter-ionic distances decrease, spin–spin communication is enhanced and we expect that the spin flip time τ_R will decrease as well ($\tau_R \ll 1/\omega_L$), leading to a progressively more symmetric HS doublet (see figures 10(a) and (b)). Also, the pressure induced distortion increases the axial crystal field splitting (i.e., the separation of the Kramers doublets) so the excited states ($S_z = \pm 3/2, \pm 5/2$) are less likely to be occupied. Consequently the shorter relaxation times associated with $S_z = \pm 1/2$ become dominant, resulting in a more symmetric resonance profile with increasing P. That is, the behaviour upon increasing P is similar to the behaviour upon lowering T, where spin–spin relaxation behaviour of the ionic ground state $S_z = \pm 1/2$ is dominant. Focusing now on the LS pressure regime (figure 10(c)) it may be noted that the (wider split) LS doublet is also asymmetric. If this asymmetry of the LS profile is due to relaxation effects associated with the (only possible) $S_z = \pm 1/2$ Kramers doublet, then it may best be explained by some structural change having occurred on conversion from the HS to LS state. Blume and Tjon [16] have shown that, in the fast spin–spin relaxation time regime, when there is a reorientation of the EFG (from parallel to perpendicular) with respect to the magnetic quantization (z) axis, there will be a reversal in the asymmetry of the quadrupole doublet to a case where the low velocity line is less intense in the resonance profile. If such an EFG reorientation accounts for the switching of the asymmetry of the HS resonance profile (figure 10(a)) to that of the LS profile (figure 10(c)), then this is probably associated with a structural rearrangement due to the HS/LS transition. It may be noted that the asymmetry of the LS profile is independent of temperature (see the right panel of figure 11) and this perhaps excludes the possibility that it arises from the Goldanskii–Karyagin effect [17] (anisotropy of the Debye–Waller factor), which is manifested as a (weakly) temperature dependent asymmetric quadrupole split resonance profile.

In the decompression sequence starting from the highest pressure of ∼20 GPa, it was found that the material was still completely LS at 3.3 GPa. Figure 12 is thus a clear indication that there is hysteresis behaviour in the compression/decompression cycles. After decompression from ∼20 GPa to ambient conditions, there is a significant difference in the spectrum of the complex in comparison to the original data. This may suggest that there has been some form of structural change induced by the very large strain at high pressure. Some of the LS state may be 'locked in' by the structural changes and this allows the complex to retain some LS character. Alternatively the effects of residual strain in the crystallites could be responsible for local lattice deformations and an associated change in the resonance profile, similar to the behaviour at low pressure values upon compression; see figure 10(a). Note that to describe the recovered system as intermediate spin would be incorrect. Intermediate spin complexes have a larger EFG than HS or LS complexes and one would expect a quadrupole doublet with $\Delta E_Q \sim 3$ mm s^{-1} if the complex was indeed in the intermediate state.

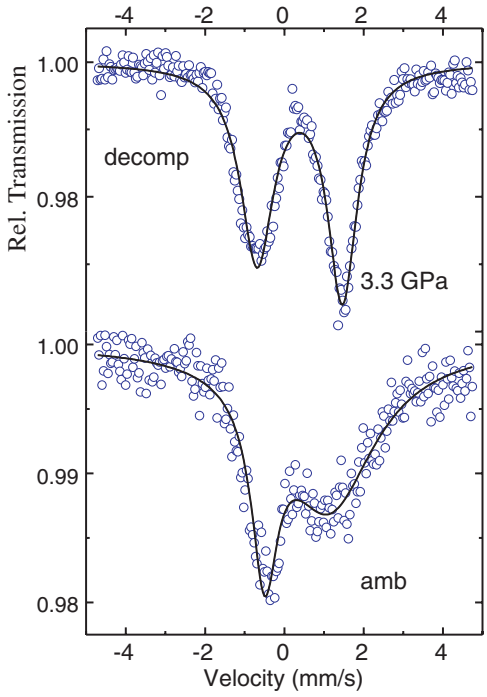

Figure 12. Mössbauer spectra recorded upon decompression from the highest pressure of 19.5 GPa. Note that at 3.3 GPa pressure release, the compound is still LS, unlike the behaviour in the compression sequence, thus suggesting that there is some pressure hysteresis.

5. DFT calculations of the spin states of [Fe(TPP)(NCS)] and possibilities for a single-molecule magnetic switch

5.1. DFT calculations of spin state geometries and energies

DFT calculations (B3LYP functional [18], LACVP** basis set [19], medium grid) were performed with Jaguar 4.0 [20] running on a Compaq AlphaStation DS20e. The LACVP** basis set uses effective core potentials for the elements K–Cu, Rb–Ag, Cs–La and Hf–Au. Second and third row s- and p-block elements are described by Pople's 6-31G** basis set [21]. The total energies $E_{el}(0)$ for the HS and LS complexes were calculated after full geometry optimizations. The converged DFT wavefunctions for each complex were analysed with the Weinholds NBO 4.M. program [22] which uses the first-order reduced density matrix of the wavefunction to obtain natural atomic orbitals (NAOs) and natural electron populations for the system. The input files for the results shown in figure 13, i.e., geometry optimizations, contained coordinates from the x-ray structure of the synthesized compound [Fe(TPP)(NCS)].

All input files contained only the basic core of the porphyrin part of the molecule (phenyl groups replaced with hydrogens to give a porphine (P) derivative). This was done to minimize calculation times and assumes that the phenyl groups do not have a significant effect on the electron interactions between the metal and the thiocyanate ligand.

For the [Fe(TPP)(NCS)] five-coordinate iron (III) compound (figure 2), DFT calculations predict that the angle between the metal and the first two atoms of the thiocyanate ligand is nearly linear. The calculation was performed with the iron atom in the 3+ oxidation state with a multiplicity of 6, indicative of a HS state {2(5/2) + 1}. We observe a similar nearly linear angle of 175.0° in the room temperature solid state structure. The HS Fe(III) ion is displaced out of the plane of the porphyrin towards the ligand by 0.55 Å in the x-ray determined structure (figure 2) and DFT calculations predict an almost identical displacement of 0.57 Å.

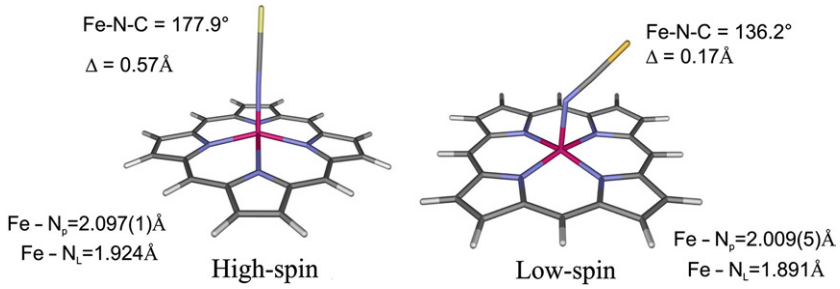

Figure 13. Comparison of DFT optimized (energy minimized) structures for the HS and LS electronic states. Phenyl groups, hydrogen atoms and counterions have been omitted for clarity (and in the calculations). Pertinent bonding distances and angles have also been indicated; Δ is the displacement of Fe out of the porphyrin plane.

The geometry optimized structure also shows the ideal conformation of the porphyrin ligand with a slight doming effect due to the size and displacement of the Fe(III) ion (figure 13). The symmetry of the DFT core geometry is exact C_{4v} symmetry; that of the x-ray structure is less regular, consistent with crystal packing effects on the core conformation.

Calculations were also performed in order to establish the differences in energy of DFT optimized HS and LS structures. Clearly, it is important to know what the proposed crystal structure of the LS compound would be and how different it would be in energy from the ionic spin sextet ($S = 5/2$ HS state). Figure 13 depicts the results of this calculation. Here it must be noted that DFT calculated energies for a particular compound could be meaningless because they may not be close enough to the real energy of the system (without complicated corrections). However, with two isomeric structures the energy difference between the two forms can be reliably used for comparison purposes.

The calculation reveals an energy difference of 19.6 kcal mol^{-1} between the HS and LS states for [Fe(P)(NCS)]. This energy is substantial but it is not an overly large energy penalty. It mainly reflects the spin pairing energy penalty and the coordination sphere adjustments that attend the switch to the LS state. It is also noteworthy that in the actual solid state structure of [Fe(TPP)(NCS)], there are also the *meso*-phenyl groups attached to the porphyrin which could have an influence on the energy gap between the HS and LS states, depending on the geometry changes that are needed to change between spin states.

The most interesting feature of this DFT result is that the NCS ligand is not linearly bound to the LS Fe(III) ion. This indicates that there are electronic interactions in the LS state that are not present in the HS state. It appears that in a Fe(III) LS state, the bent form of the axial ligand is preferred, because in this form it is a stronger field ligand than when it is linearly bound. This bending of the axial ligand is probably the energetically favoured geometry when there is increased packing of the molecules and associated enhanced inter-molecular interactions, at high pressure.

Interestingly, there is a structure published by Scheidt and co-workers [23] that has a bent NCS ligand (Fe–N–C = 155.6(3)°) coordinated with LS Fe(III), [Fe(TPP)(py)(NCS)]. The bend in this compound was ascribed to packing interactions [23].

One other point to note is that the DFT calculations predict a substantial decrease (∼0.4 Å) in the displacement of the Fe(III) ion from the porphyrin plane on converting to the LS state, which causes a ∼2.5° increase in the N_p–Fe–N_p angle and a ∼0.1 Å decrease in the Fe–N_p bond distance, as would be expected for a configuration in which the $d_{x^2-y^2}$ orbital electron population is formally zero.

5.2. Single-molecule switching in metalloporphyrins

In recent work a single-molecule switch has been realized in a Cu-tetra-3,5 di-tertiary-butyl-phenyl porphyrin (Cu-TBPP), based on the rotation of a di-butyl-phenyl (DBP) leg (ligand) placed in a tunnel junction. The electronic characteristics of such a hybrid nanoswitch have been studied with an STM [24]. In its 'ON' state, the axis of a DBP leg was manipulated by the STM tip to be perpendicular to the copper porphyrin plane. In its 'OFF' state, the orientation was parallel, resulting in a low tunnelling current through this leg. The state of this switch has also been controlled by using the tip apex of an AFM to push and therefore rotate one of the four legs of the Cu-TBPP molecule. This has permitted a unique identification of the forces and energies required to rotate a single (C–C) bond in the molecule, so as to obtain switching behaviour.

In a similar vein we suggest that the iron-based porphyrin [Fe(TPP)NCS] may be used as a single-molecule *magnetic* switch, provided that STM/AFM manipulation of the *axial* (NCS) ligand can be readily achieved. By bending the axial ligand away from linear, the magnetic state of the molecule can be 'toggled' between the high moment (HS) and low moment (LS) state, e.g., to represent bit 1 and bit 0 states in nanomemory arrays; see figure 13.

Acknowledgment

Funding for this work was derived from the NRF (Pretoria—SA) and this is acknowledged with gratitude.

References

[1] Kwok K S and Ellenbogen J C 2002 *Mater. Today* **5** 28
[2] Gutlich P, Gaspar A B, Ksenofontov V and Garcia Y 2004 *J. Phys.: Condens. Matter* **16** S1087
[3] Money V, Elhaik J, Evans I R, Halcrow M A and Howard J A K 2004 *Dalton Trans.* **65** 65
[4] Khan O and Martinez C J 1998 *Science* **279** 44
[5] Milgrom L R 1997 *The Colours of Life: An Introduction to the Chemistry of Porphyrins and Related Compounds* (Oxford: Oxford University Press)
[6] Scheidt W R 2000 *Porphyrin Handbook* vol 3, ed K M Kadish, K M Smith and R Guilard (New York: Academic) chapter 16
[7] Hearne G R, Pasternak M P and Taylor R D 1994 *Rev. Sci. Instrum.* **65** 3787
[8] Blume M 1967 *Phys. Rev. Lett.* **18** 305
[9] Harris G 1968 *J. Chem. Phys.* **48** 2191
[10] Blume M 1965 *Phys. Rev. Lett.* **14** 96
[11] Iizuka T and Kotani M 1969 *Biochim. Biophys. Acta* **181** 275
[12] Iizuka T and Yonetani T 1970 *Adv. Biophys.* **1** 157
[13] Zhang Y, Hallows W A, Ryan W J, Jones J G, Carpenter G B and Sweigart D A 1994 *Inorg. Chem.* **33** 3306
[14] Pearson N 2002 Structural and physical studies on thiocyanate complexes of metalloporphyrins *MSc Dissertation* School of Chemical and Physical Sciences, University of Kwazulu-Natal, Pietermaritzburg, SA
[15] Boldyreva E V 2003 *J. Mol. Struct.* **647** 159
[16] Blume M and Tjon J A 1967 *Phys. Rev.* **165** 446
[17] Goldanskii V I, Makarov E F and Khrapov V V 1963 *Phys. Lett.* **3** 344
[18] Becke A D 1993 *J. Chem. Phys.* **98:7** 5648
[19] Hay P J and Wadt W R 1985 *J. Chem. Phys.* **82** 299
[20] *Jaguar Version 4.0* 2000 (Portland, OR: Schrödinger, Inc.)
[21] Francl M M, Pietro W J, Hehre W J, Binkley J S, Gordon M S, Defrees D J and Pople J A 1982 *J. Chem. Phys.* **77** 3654
Rassolov V A, Pople J A, Ratner M A and Windus T L 1998 *J. Chem. Phys.* **1223** 109
[22] Glendening E D, Badenhoop J K, Reed A E, Carpenter J E and Weinhold F 1999 *NBO 4.M.* (Madison, WI: Theoretical Chemistry Institute, University of Wisconsin)
[23] Scheidt W R, Mondal J U, Eigenbrot C W, Adler A, Radonovich L J and Hoard J 1986 *Inorg. Chem.* **25** 795
[24] Moresco F, Meyer G, Rieder K-H, Tang H, Gourdon A and Joachim C 2001 *Phys. Rev. Lett.* **86** 672